JOURNAL OF MATERIALS PROCESSING TECHNOLOGY 198 (2008) 372–380

journal homepage: www.elsevier.com/locate/jmatprotec

Numerical simulation of the lubricant performance in tube hydroforming

*Mariela Luege, Bibiana M. Luccioni**

Instituto de Estructuras, Universidad Nacional de Tucumán, CONICET Country Las Yungas, 4107 Yerba Buena, Tucumán, Argentina

ARTICLE INFO

Article history:
Received 26 November 2006
Received in revised form 6 July 2007
Accepted 11 July 2007

Keywords:
Hydroforming process
Lubrication
Friction law
Computational contact mechanics

ABSTRACT

Due to the high pressures that are involved in tube hydroforming processes, high values of the friction forces are developed and, therefore, lubricants are usually employed to increase the formability of the workpiece. However, different lubrication regimes are observed along the different forming zones which vary with the lubricant layer thickness, applied load and sliding velocity. A constitutive relation that captures these features of tribology between two surfaces separated by an atomically thin layer of lubricant molecules is proposed in this paper.

The model defines the tangential stress as sum of two contributions: one purely frictional and the other one of viscous type. The frictional contribution depends on the contact between the asperities, whereas the viscous contribution is described by means of an effective viscosity coefficient that accounts for the thin lubricant layer separating such asperities. The model is implemented in a FE code and validated with a pear-shape expansion test. Comparisons with the Coulomb's law are also presented showing a better performance of the proposed model.

1. Introduction

The control of the interface conditions between the die cavity and the work piece plays a crucial role in the design process of tube hydroforming (hereafter THF for brevity) (Dohmann and Hartl, 1997; Ahmetoglu and Altan, 2000; Vollersten et al., 1999). Because of the high contact pressures, necessary to expand the tube in the die cavity, and the large contact surface that is involved, very high friction forces can be generated. These forces can adversely affect the process in different ways, such as limiting the relative movement between tube and die, specially for long tube components, leading to a tube thinning in the expansion zone caused by the lack of axial force, and affecting the surface integrity of the tube. The development of lubrication systems that enhance the tribological performance in THF processes can lead to an optimal utilization of this technology in the manufacture of complex parts (Geiger and Dal Bó, 2005; Geiger et al., 2005; Ngaile et al., 2004a).

Different regimes of lubrication are developed along the different forming zones, depending on the sliding velocity, pressure and contact surface conditions. Progresses in measuring tribology of confined thin lubricant fluids (Israelachvili, 1992) have allowed more reliable representations of the above conditions, by means, for instance, of the boundary lubrication map (see Fig. 1). The increasing use of numerical methods to simulate forming processes demands the inclusion of more physics, not only at the material level but also in the modelling of the interface, in order to obtain more realistic numerical simulations.

* *Corresponding author*. Tel.: +54 381 4364087; fax: +54 381 4364087.
E-mail address: bluccioni@herrera.unt.edu.ar (B.M. Luccioni).
0924-0136/$ – see front matter © 2007 Elsevier B.V. All rights reserved.
doi:10.1016/j.jmatprotec.2007.07.040

Nomenclature

A_v	sliding velocity when $\mu_0 = \mu_k$
D	lubricant's film thickness
D_0	microcontact's refreshed distance
D_{max}	viscous thickness threshold
D_{min}	frictional thickness threshold
f	real contact area function
g	gap function
g_T	total sliding distance
g_T^e	reversible sliding distance
g_T^p	permanent sliding distance
K_N, K_T	penalty parameters
$\mathcal{L}$	lie derivative
m	material parameter (Ruina, 1983)
$t_N v$	normal contact stress
$\boldsymbol{t}_T$	tangential contact stress
$\boldsymbol{T}$	nominal contact traction
V_{CR}	critical velocity

Greek letters

α	frictional/viscous weighting coefficient
φ_t^i	deformation mapping of the body i at time t
τ_0	microcontact's refreshed time
η	effective viscosity
η_b	lubricant's bulk viscosity
λ	plastic multiplier
μ_0	steady state friction coefficient
μ_s	static friction coefficient
μ_k	kinetic friction coefficient
v	outward normal
θ	average age of contact

In the boundary lubrication map the friction force F is defined as a function of the sliding velocity V and it is represented in terms of a family of curves parameterized by the lubricant film thickness D or the applied normal load L. Three zones can be observed in these curves: viscous, intermediate and pure frictional. The viscous regime, generally obtained with relatively thick lubricated surfaces and small values of L, is characterized by a viscous response with constant viscosity

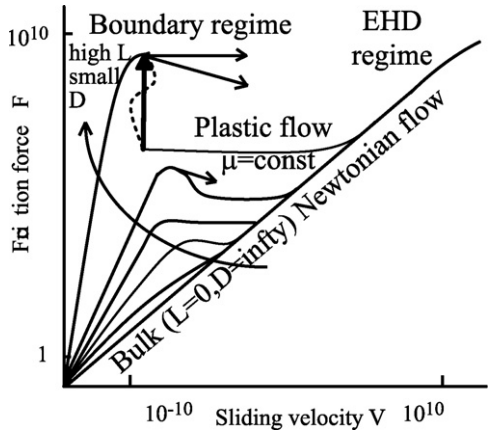

Fig. 1 – Example of boundary lubrication map proposed in (Luengo et al., 1996).

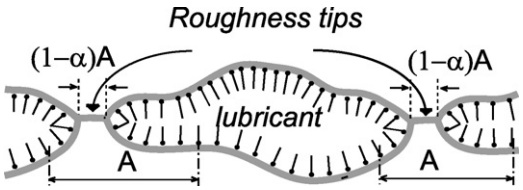

Fig. 2 – Micromechanical model of the contact between solid surfaces in the presence of a boundary film (Tabor, 1952).

equal to the bulk fluid viscosity η_b of the lubricant. The pure frictional regime (Hsu, 1997; Ko, 2003) takes place in presence of very high loads L and low film thicknesses D. In this regime, the friction force reaches a peak coincident with the static friction force, which remains roughly constant with increasing velocity until a pure viscous regime is obtained, for a certain critical D-dependent velocity V_{CR}. In the intermediate region, also known as boundary lubrication regime, the transition to the bulk viscous regime is smooth and signed by the sliding velocity V_{CR} depending on D (or on L). The boundary layer films are characteristic of the high load and intermediate regimes, where the surface asperities penetrate the lubricant layer and are separated from each other, at their tips, only by films of molecular thickness as depicted in Fig. 2 (Tabor, 1952).

The latter considerations on the phenomenology at the microlevel scale give information about how, in presence of boundary lubricant, the load is supported by the lubricant film and by minute surface junctions. As a result, two contributions can be identified: the force $(1-\alpha)At_T^m$ required to shear the surface junctions (with $(1-\alpha)$ the fraction of the area A over which surface junctions are formed and t_T^m the shear strength of the metal) and the force $A\alpha t_T^l$ required to shear the lubricant film, with t_T^l the shear strength of the lubricant itself, i.e.:

$$F = A[(1-\alpha)t_T^m + \alpha t_T^l]. \quad (1)$$

Under these conditions, if the Coulomb's law is adopted for the definition of the friction coefficient, the relative importance of the two mechanisms should be somehow accounted for. As a result, different friction coefficients for the different forming zones (Vollersten and Plancak, 2002; Plancak et al., 2005) which should then be changed adaptively in the finite element simulations of THF processes (Geiger and Dal Bó, 2005) should be considered.

With the objective of providing a unitary description of the tribological conditions that might occur in a THF process, a friction law that embodies the salient features of the boundary lubrication map is proposed in this paper. Motivated by the above mentioned mechanisms, which take place at the micro scale, the model defines the friction force as the sum of two contributions, a pure frictional and a pure viscous one, weighted by coefficients depending on the lubricant film thickness D and the sliding relative velocity V by means of a control variable $\alpha \in [0,1]$. The extreme conditions of pure frictional and pure viscous regime are achieved for $\alpha = 0$ and $\alpha = 1$, respectively. The model is formulated in the framework of the thermodynamics of irreversible processes with internal variables and depends on rate and state variables. The

rate variable is the sliding velocity, whereas the two state variables, represented by the irreversible sliding distance and the average age of contact, are introduced to capture all memory dependent effects (Ruina, 1983; Carlson and Batista, 1996; Laursen, 2002). The calibration of the proposed model requires few experimental parameters which must be obtained from the boundary lubrication map.

After this introduction the remaining part of the paper is organized as follows. In Section 2, after a brief recall of contact mechanics, the new friction law is introduced together with the definition and evaluation of the parameters required for its calibration. Section 3 reports the use of the proposed friction law in the FE simulation of a pear-shaped expansion test. This is a model test designed for the ranking of lubricants (Ngaile et al., 2004a,b). For this example, the proposed contact law is compared with the classical Coulomb's friction law and it is shown to reproduce quite well the experimental results of Ref. (Ngaile et al., 2004b) unlike the Coulomb's law. Concluding remarks are presented in Section 4.

2. The contact model for lubricated and dry interface conditions

The constitutive relation that describes the distinguishing features of the tribology of surfaces separated by a few molecular layers of lubricant is presented in this Section. It is worth noting that the tangential stress should depend on details associated with the microscopic properties of the lubricant. However, when the system is sufficiently large to be self-averaging, an effective dependence of the friction on macroscopic variables such as time, irreversible sliding distance and sliding velocity can be postulated.

2.1. Hypotheses and notations

Let β^1 and β^2 denote the two bodies that come into contact, and denote by $\mathbf{x} = \varphi_t^1(\mathbf{X})$ and $\mathbf{y} = \varphi_t^2(\mathbf{Y})$ the corresponding deformation mappings at time $t \in I$, where $I = [0,T]$ is the time interval of interest. The boundary Γ^i for $i = 1,2$ of each body can be partitioned in three parts: $\Gamma^i_{\mathbf{u}}$ and Γ^i_{σ} have prescribed displacements and tractions, respectively; whereas Γ^i_c is the part of the boundary which is expected to come into contact with the other body at a certain instant $t \in I$ and is where both the contact and friction conditions must be formulated (Curnier, 1984).

In order to establish the contact conditions that enforce the physical requirement of impenetrability and compression interaction between the two bodies, the gap function is introduced as

$$g(\mathbf{X}, t) = -\boldsymbol{\nu}[\varphi_t^1(\mathbf{X}) - \varphi_t^2(\bar{\mathbf{Y}})] \tag{2}$$

with $\bar{\mathbf{y}} = \varphi_t^2(\bar{\mathbf{Y}})$ being the closest point of $\varphi_t^2(\Gamma_c^2)$ to $\varphi_t^1(\mathbf{X})$ and $\boldsymbol{\nu}$ the outward normal to the surface $\varphi_t^2(\Gamma_c^2)$ at $\bar{\mathbf{y}}$.

The full description of the kinematics of the contact is completed by introducing also the tangential relative velocity $\mathcal{L}_v \boldsymbol{g}_T$. This is defined as the Lie derivative of the tangential slip distance $\boldsymbol{g}_T$, for it is an objective quantity (Marsden and Hughes, 1994; Laursen, 2002).

2.2. Constitutive contact equations

The nominal contact traction on $\boldsymbol{X}$ is decomposed in its normal $t_N \boldsymbol{\nu}$ and tangential $\boldsymbol{t}_T$ component as follows:

$$\boldsymbol{T}(\boldsymbol{X}, t) = -\boldsymbol{t}_T(\boldsymbol{X}, t) + t_N(\boldsymbol{X}, t)\boldsymbol{\nu}. \tag{3}$$

Considering the contact area Γ_c as a material boundary (Fremond, 1987), the state laws consist of normal contact conditions that involve t_N and g, and friction conditions that relate $\boldsymbol{t}_T$ to $\boldsymbol{g}_T$.

2.2.1. Normal contact conditions

To enforce the impenetrability constraint, the following conditions are given:

$$g \le 0, \quad t_N \ge 0, \quad t_N g = 0. \tag{4}$$

The first condition states that the two solids can either be separated from each other ($g < 0$), or in contact to each other ($g = 0$), but they cannot penetrate to each other. According to the second condition, adhesion is not allowed (i.e. $t_N < 0$ is not possible) whereas, according to the last one, either it is $t_N = 0$ when $g \neq 0$ or $t_N > 0$ for $g = 0$.

Given the unilateral character of the first two conditions, the resulting problem is nonsmooth. A regularised version, useful for the numerical simulation, is obtained by assuming $t_N = K_N \langle g \rangle_+$ with K_N a penalty parameter that can be interpreted as normal stiffness of the asperities and $\langle \cdot \rangle_+ = \max\{0, \cdot\}$. In the regularised problem, some penetration of the solid into the obstacle will be therefore allowed.

2.2.2. Friction conditions

To describe the frictional response an additive decomposition of the total slip distance $\boldsymbol{g}_T$ in an elastic $\boldsymbol{g}_T^e$ and a permanent component $\boldsymbol{g}_T^p$ is assumed, that is, $\boldsymbol{g}_T = \boldsymbol{g}_T^e + \boldsymbol{g}_T^p$. The tangential stress $\boldsymbol{t}_T$ is accordingly defined as the sum of two contributions: a pure frictional, which depends on the asperities elastic deformation $\boldsymbol{g}_T^e$, and a pure viscous contribution, which depends on the relative sliding velocity $L_v \boldsymbol{g}_T$ as follows:

$$\boldsymbol{t}_T = (1 - \alpha) K_T \boldsymbol{g}_T^e + \eta(\alpha) L_v \boldsymbol{g}_T. \tag{5}$$

In Eq. (5), K_T describes the tangential stiffness of the asperities, whereas $\eta(\alpha)$ is the effective viscosity of the lubricant film. The expression of η is given in Section 2.2.3 and depends on the control parameter α, with $\eta(0) = 0$ and $\eta(1) = \eta_b$. The coefficient $\alpha \in [0,1]$ averages the viscous and frictional contribution and depends on the sliding velocity $|L_v \boldsymbol{g}_T|$ and on the lubricant layer thickness D with the following expression:

$$\alpha = \begin{cases} \min\left\{ \left(\dfrac{\langle D - D_{\min} \rangle_+}{D_{\max} - D_{\min}} \right), 1 \right\} & \text{if } |L_v \boldsymbol{g}_T| < V_{CR}(D), \\ 1 & \text{if } |L_v \boldsymbol{g}_T| \ge V_{CR}(D). \end{cases} \tag{6}$$

In Eq. (6) the critical velocity $V_{CR}(D)$, which marks the passage from a frictional/viscous regime to a pure viscous one, depends on the lubricant film thickness D and must be evaluated once the boundary lubrication map is known from the experiments; D_{max} and D_{min} are the maximum

and minimum film thicknesses signing a pure viscous (for $D \geq D_{max}$) and pure frictional regimes (for $D \leq D_{min}$), respectively, and are also quantities known from the experiments. The tangential stress equals, therefore, the pure frictional one when $D \leq D_{min}$ and $|L_v \boldsymbol{g}_T| < V_{CR}$, and the pure viscous one when $D \geq D_{max}$ or $|L_v \boldsymbol{g}_T| \geq V_{CR}$. For the other combinations of $|L_v \boldsymbol{g}_T|$ and D, an intermediate regime is obtained where the tangential stress will depend both on the frictional behaviour between the interface asperities that are in contact and on the relative velocity $L_v \boldsymbol{g}_T$ between the interfaces.

The model is completed by introducing: (i) the evolution law of the permanent sliding distance $\boldsymbol{g}_T^p$ as

$$L_v \boldsymbol{g}_T^p = \lambda \frac{\partial F}{\partial \boldsymbol{t}_T^e}, \tag{7}$$

with λ the plastic multiplier; (ii) the consistency conditions

$$F = |\boldsymbol{t}_T^e| - f(|L_v \boldsymbol{g}_T|, \theta)\mu_0(|L_v \boldsymbol{g}_T|)t_N \leq 0, \quad \lambda F = 0, \quad \lambda \geq 0; \tag{8}$$

and (iii) the evolution of the state variable θ introduced by (Ruina, 1983) to account for the average age of contact:

$$\dot{\theta} = 1 - \theta \frac{|L_v \boldsymbol{g}_T|}{D_0} \tag{9}$$

The pure frictional part of the tangential stress is therefore controlled by a Coulomb's type yield function $\mathcal{F}$, with μ_0 the steady state friction coefficient that decreases with the sliding velocity,

$$\mu_0 = \begin{cases} \mu_k + (\mu_s - \mu_k) \exp(1) \exp\left(\dfrac{A_v^2}{\langle |L_v \boldsymbol{g}_T| - D_0/\tau_0 \rangle_+^2 - A_v^2} \right) & \text{if } |L_v \boldsymbol{g}_T| \leq A_v + D_0/\tau_0, \\ \mu_k & \text{otherwise.} \end{cases}$$

The coefficients μ_s and μ_k are the static and kinetic friction coefficients, respectively, whereas τ_0 and D_0 denote the time and the distance over which on average the microcontacts are refreshed (Ruina, 1983). The parameter A_v denotes the value of the velocity when μ_0 attains the kinetic value μ_k. The function $f(|L_v \boldsymbol{g}_T|, \theta)$ accounts for the real contact area and is defined as:

$$f(|L_v \boldsymbol{g}_T|, \theta) = 1 + m \ln\left(\theta \frac{|L_v \boldsymbol{g}_T|}{D_0} \right) \tag{10}$$

with m defined in (Ruina, 1983). The proposed model is thermodynamically consistent, that is, it satisfies the Clausius–Duhem's inequality (Luege, 2006; Luege and Luccioni, 2006).

2.2.3. *Evaluation of η*

For the evaluation of the function $\eta = \eta(\alpha)$ in (5) the boundary lubrication map of Fig. 1 along with D_{min}, D_{max} and $V_{CR}(D)$ must be assumed as given from the experiments. For one dimensional steady state sliding, with $V = L_v \boldsymbol{g}_T$ and $f(V, \theta) = 1$, Eq. (5) can be re-written as follows:

$$t_T = (1 - \alpha)\mu_0(V)t_N + \eta(\alpha)V \tag{11}$$

Shifting the origin so that sliding starts at $V = 0$, for $D \leq D_{min}$ it is assumed $\alpha = 0$. In this case Eq. (11) is represented by the line

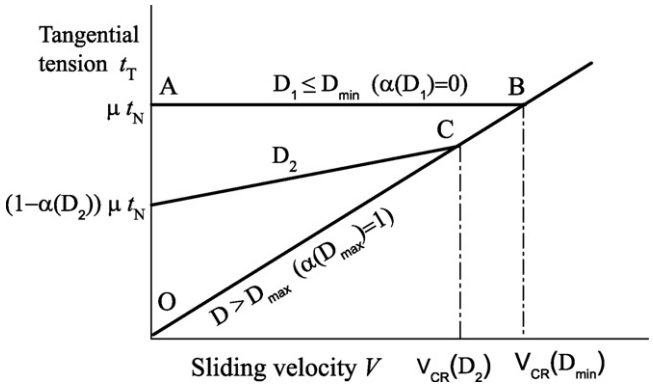

Fig. 3 – Boundary friction map obtained plotting Eq. (5) for one dimensional steady state sliding, assuming that sliding starts at $V = 0$ and $\mu_0(V) = \mu_s = \mu_k$.

AB of Fig. 3. Assuming $\alpha = 1$ when $D \geq D_{max}$, Eq. (11) is represented by the line OB of Fig. 3. For an arbitrary film thickness D_2 and $V = V_{CR}(D_2)$, the tangential stress at point C has the following expression:

$$t_{TC} = (1 - \alpha(D_2))\mu_0(V_{CR}(D_2))t_N + \eta(\alpha(D_2))V_{CR}(D_2) = \eta_b V_{CR}(D_2) \tag{12}$$

with $\alpha(D_2)$ given by Eq. (6). Eq. (12) can be therefore solved with respect to the parameter η and yields:

$$\eta(D_2) = \eta_b - (1 - \alpha(D_2)) \frac{\mu_0(V_{CR}(D_2))t_N}{V_{CR}(D_2)}. \tag{13}$$

Note that $\alpha \to 0$ for $D_2 \to D_{min}$, so that:

$$(1 - \alpha(D_2)) \frac{\mu_0(V_{CR}(D_2))t_N}{V_{CR}(D_2)} \to \frac{\mu_0(V_{CR}(D_{min}))t_N}{V_{CR}(D_{min})} = \eta_b, \tag{14}$$

which therefore yields $\eta(D_2) \to 0$. On the other hand, for $D_2 \to D_{max}$, $\alpha \to 1$ and therefore from Eq. (13), $\eta(D_2) \to \eta\ (D_{max}) = \eta_b$ is obtained. Finally, by accounting of Eq. (13), it is interesting to note that the tangential stress t_T reduces to the expression proposed in Ref. (Carlson and Batista, 1996) for 1D steady state sliding. Box 1 summarises the full constitutive model.

Box 1

Frictional/viscous contact model

Normal conditions: $g \geq 0 \quad (t_N - K_N g)g = 0 \quad t_N^e - K_N g \leq 0$

Sliding distance splitting: $\boldsymbol{g}_T = \boldsymbol{g}_T^e + \boldsymbol{g}_T^p$

Friction law: $\boldsymbol{t}_T = (1 - \alpha)K_T \boldsymbol{g}_T^e + \alpha \eta_b L_v \boldsymbol{g}_T$

$$L_v \boldsymbol{g}_T^p = \lambda \frac{\boldsymbol{t}_T^e}{|\boldsymbol{t}_T^e|} \quad \text{with } \boldsymbol{t}_T^e = (1 - \alpha)K_T \boldsymbol{g}_T^e$$

Evolution laws: $F = |\boldsymbol{t}_T^e| - (1 - \alpha)\mu_0 f t_N \leq 0 \quad \lambda \geq 0 \quad \lambda F = 0$

$$\dot{\theta} = \left(1 - \theta \frac{|L_v \boldsymbol{g}_T|}{D_0}\right) \quad f = 1 + m \ln\left(\theta \frac{|L_v \boldsymbol{g}_T|}{D_0}\right)$$

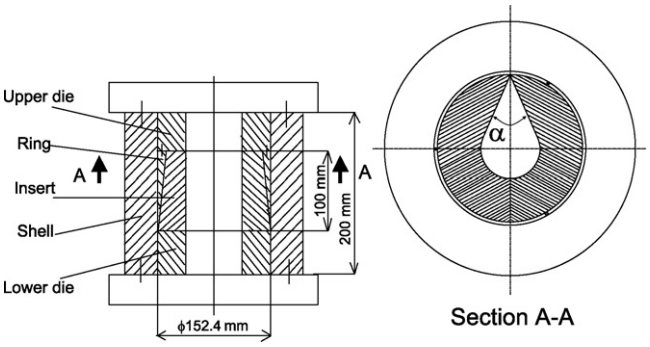

Fig. 4 – Pear-shaped expansion sub-assembly showing: die inserts, ring and housing.

Table 1 – Lubricants used in the experimental tests (Ngaile et al., 2004b) and numerical simulations

Lubricant	Properties/contents	η_b (s^{-1})
Lub A	Polimeric film and blend of non-abrasive dissimilar materials	2.0×10^{-5}
Lub B	Solid lubricant, free from chlorine and sulphur	5.0×10^{-5}
Lub C	Carbon black, graphite butoxyethanol and water	4.0×10^{-5}

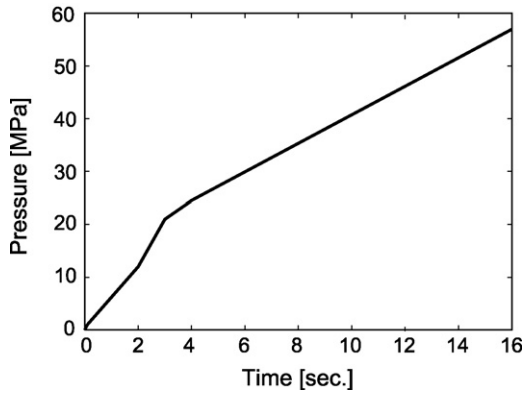

Fig. 5 – Pressure-loading path used in the pear-shaped tube expansion test (Ngaile et al., 2004b).

3. Finite element simulations

An Euler scheme with a predictor/corrector step is adopted for the numerical integration of the proposed model. The model is implemented in the explicit finite element code STAMPACK®. In order to validate the proposed model, the pear-shaped tube expansion test is next considered where the proposed model is compared with the Coulomb's law. The parameters D_0/τ_0, D_0, m, A_v, D_{max} and D_{min}, required for the calibration of the proposed friction law, are taken from the experimental observations of (Luengo et al., 1997, 1996) considering different film thicknesses (see also Ref. (Luege, 2006) for more details). The critical velocity parameter is

Table 2 – Model parameters for the proposed contact law

$K_N = K_T$	μ_s	μ_k	D_0/τ_0 (m/s)	D_0 (nm)	m	A_v (m/s)	D_{max} (nm)	γ
0.001	0.6	0.1	0.3	1.0×10^{-6}	0.1	2.5	250	0.01

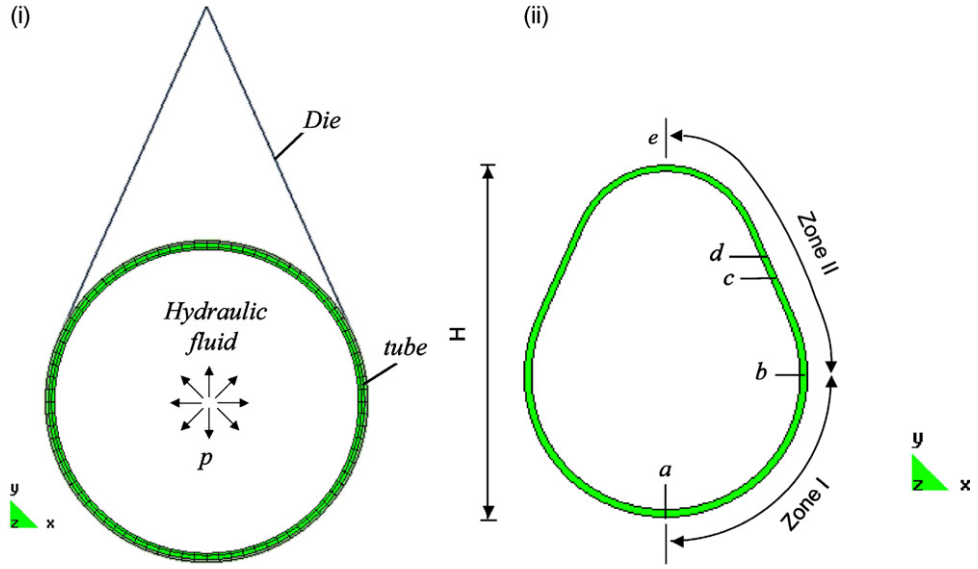

Fig. 6 – (i) Finite element model of the tubular specimen placed in a pear-shape die under internal pressure *p*. (ii) Deformed tubular specimen.

determined as $V_{CR}(D) = \sqrt{\gamma D_{max}/\eta_b D}$, where the constant γ is fitted to the experimental results.

3.1. *Pear-shaped tube expansion test*

The pear-shaped tube expansion test is described in Ref. (Ngaile et al., 2004a) to evaluate the performance of THF lubricants at the expansion zone. Fig. 4 shows the geometry and configuration of the expansion tool (Ngaile et al., 2004b). The test consists of pressurizing hydraulic fluid inside a tubular specimen, which is placed inside the die inserts, until the required interface pressure is reached. A particular feature of the pear-shaped die geometry is that the material is confined to flow in only one direction. Experimental tests carried out in Ref. (Ngaile et al., 2004b) refer to SS304 tubular specimens of 250 mm in length, 57 mm in diameter and 1.6 mm wall thickness. The lubricants reported in Table 1 and also the condition of no lubricant, hereafter referred to as no-Lub, are used.

3.1.1. *FE model*

Given the symmetry of the model, only a 2D radial section of the tube is modelled. The FE model consists of 240 quadrilateral bilinear plane strain FEs. The stainless steel tube is

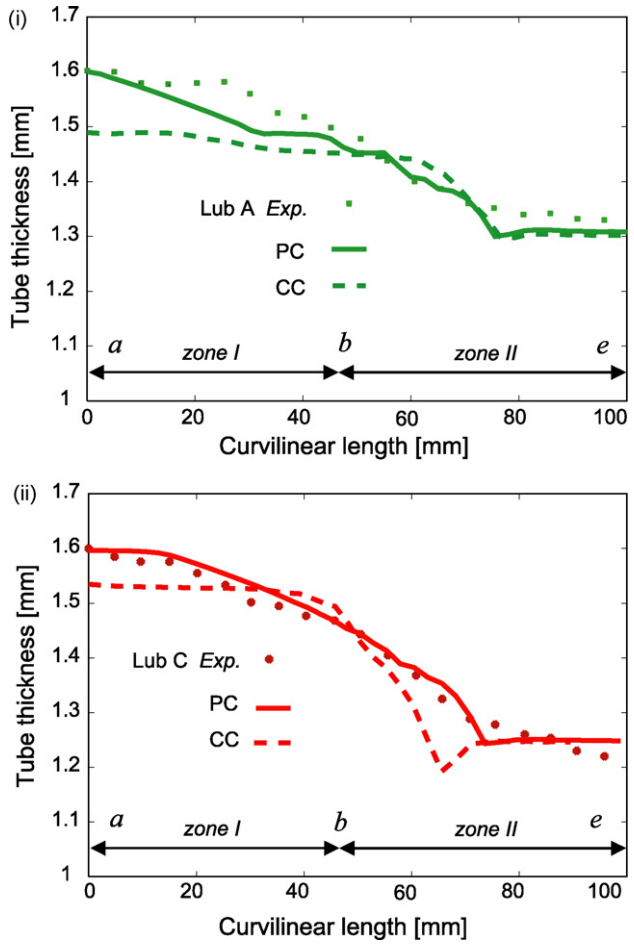

Fig. 7 – Wall thickness distribution numerically obtained using the classical Coulomb's law (CC) and the proposed contact law (PC), together with the experimental results (Exp) (Ngaile et al., 2004b), for the cases: (i) Lub A, (ii) Lub C.

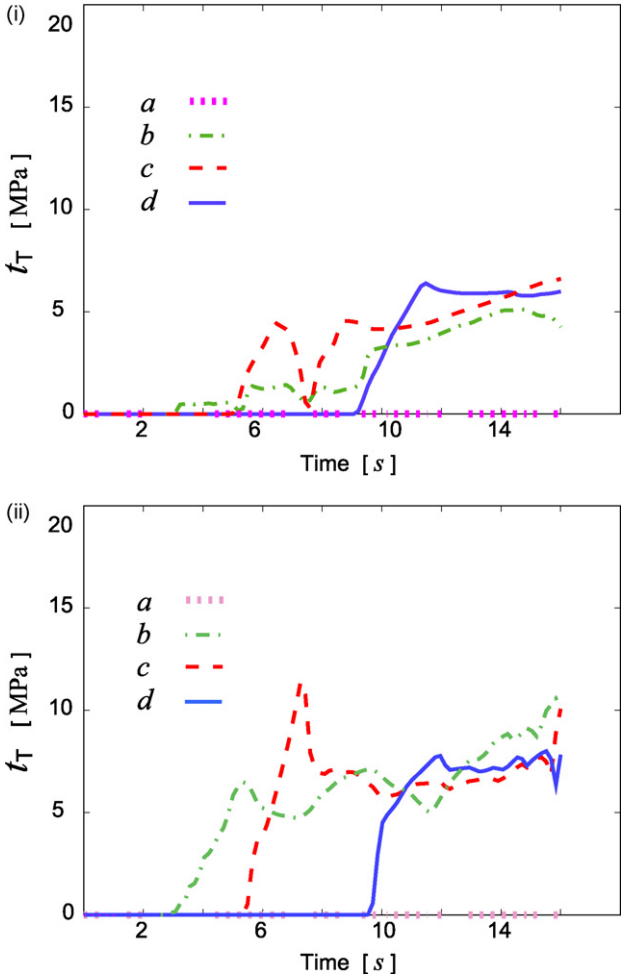

Fig. 8 – Tangential contact stress evolution during the forming process, at the points *a*, *b*, *c* and *d* of the tube–die interface defined in Fig. 6. (i) Lub A with CC model; (ii) Lub A with PC model.

modelled with von Mises elastoplasticity and the nonlinear isotropic hardening law $\sigma_y = C_0(\epsilon_0 + \epsilon)^{C_N}$, assuming Young's modulus $E = 1.93 \times 10^5$ MPa, Poisson's coefficient $\mu = 0.350$, $C_0 = 1.55 \times 10^3$ MPa, $C_N = 0.624$ and $\epsilon_0 = 0.6 \times 10^{-1}$ (Ngaile et al., 2004b).

The die is modelled by a linear interface element that imposes unilateral contact conditions, whereas the friction conditions are modelled either with the classical Coulomb's law or with the constitutive model for lubricated and dry interface conditions proposed in Section 2. When the Coulomb's law is used, three friction coefficients μ equal to 0.1, 0.3 and 0.6 are considered, as suggested in Ref. (Wriggers, 2002) for a metal/metal interface. Table 2 summarises the parameters that have been adopted for the proposed model. For the case of lubricated surfaces, a layer thickness of $D = 180$ nm is used, whereas for the dry case $D = D_{min} = 0$ is assumed.

The time evolution of the applied hydraulic pressure is reported in Fig. 5, whereas Fig. 6 depicts the FE model together with its deformed final mesh.

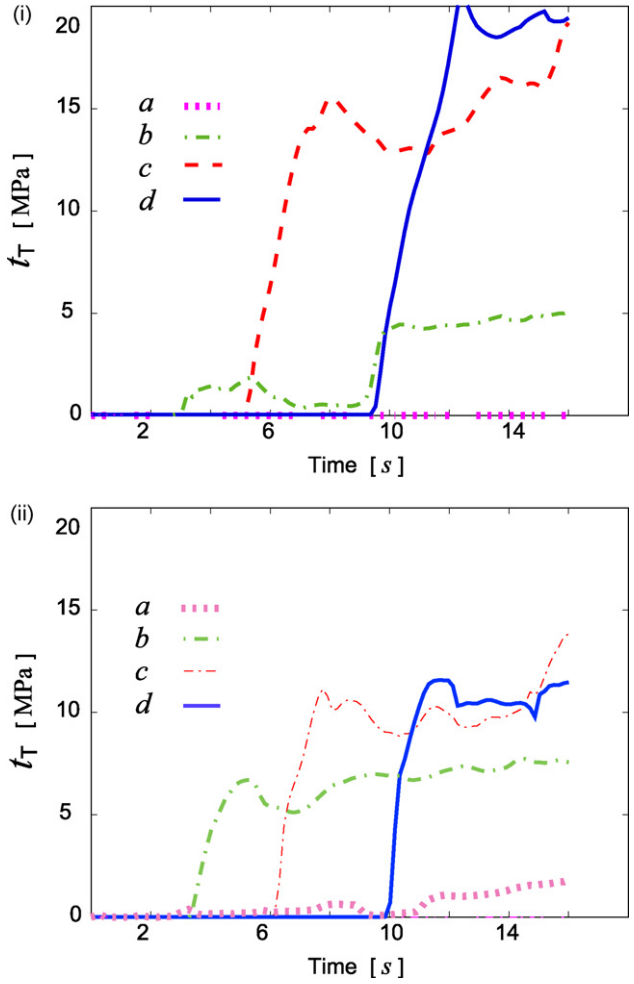

Fig. 9 – Tangential contact stress evolution during the forming process, at the points *a*, *b*, *c* and *d* of the tube–die interface defined in Fig. 6. (i) Lub C with CC model; (ii) Lub C with PC model.

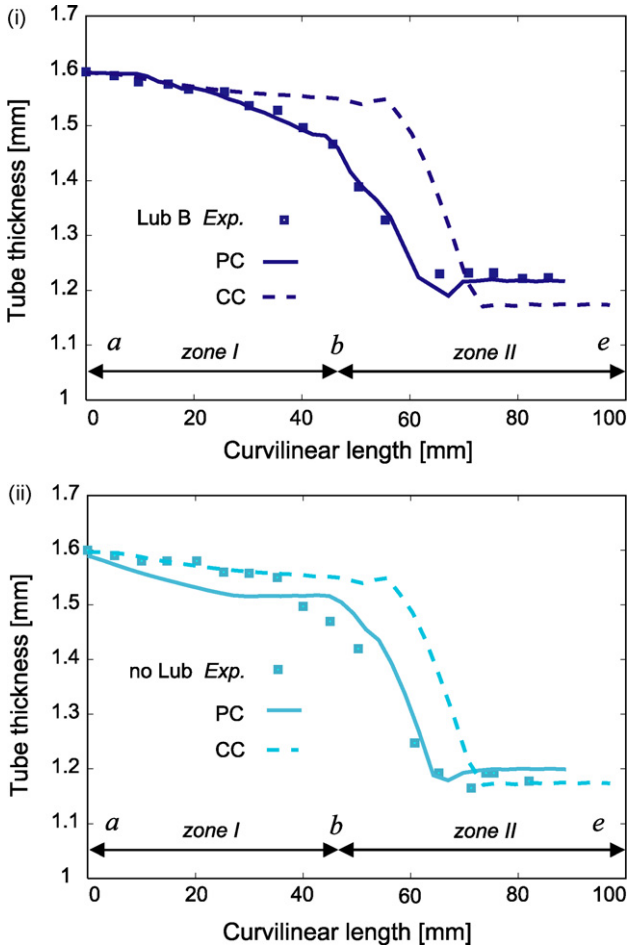

Fig. 10 – Wall thickness distribution numerically obtained using the classical Coulomb's law (CC) and the proposed contact law (PC), together with the experimental results (Exp) (Ngaile et al., 2004b), for the cases: (i) Lub B and (ii) no-Lub.

3.1.2. *Numerical versus experimental results*

The experimental tests carried out in Ref. (Ngaile et al., 2004b) show the existence of two zones in the wall thickness distribution of the pear-shaped specimens: zone I where the tube is in contact with the die, and zone II where the tube is free to expand to the apex (see also Fig. 6(ii) for the deformed configuration). Comparison of the experimental observations with the numerical ones obtained using the proposed contact law (hereafter referred to as PC model) and the classical Coulomb's law (next referred to as CC model) are shown in Figs. 7–11.

For the lubricants A and C, whose properties are given in Table 1, Fig. 7(i) and (ii) show the wall thickness distribution numerically obtained using the PC and the CC model, and the comparison with experimental results. See Fig. 6(ii) for the definition of points *a*, *b* and *e*. Fig. 7 shows that the thickness distribution obtained with the PC model decreases almost linearly along zone I and zone II, following the experimental observations. On contrary, the use of the CC model yields a constant thickness value around 1.5 mm along the zone I.

For a better interpretation of these results, the time evolution of the module t_T of $\mathbf{t}_T$ at the points *a*, *b*, *c* and *d*, along the tube–die interface, is plotted in Figs. 8 and 9. For both Lub A and Lub C, the strong thinning of the tube near zone I can be attributed to the initial low tangential contact stress t_T obtained with the CC model, compared to the one obtained

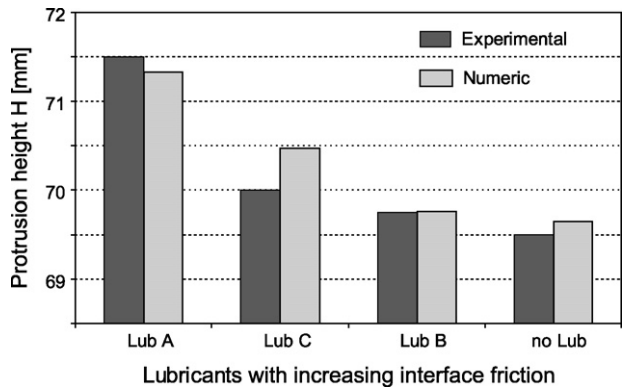

Fig. 11 – Protrusion height *H* of the tube for 57 MPa internal pressure and using different types of lubricants. Comparison between numerical and experimental results.

with the PC model. The tangential contact stress t_T for the PC model takes almost a uniform value during the forming process, unlike for the CC model. Furthermore, the PC model gives higher friction values than the CC model where slow sliding velocities take place (see the evolution of the tangential stress at points *a* and *b*). On contrary, near the expansion zone, i.e. at points *c* and *d*, lower friction values are obtained with the PC compared to the CC model. This difference between the two models appears because, unlike the CC model, the PC model is able to describe the pure viscous behaviour resulting from an increase of sliding velocity (melting effect).

For the lubricant B and in the case of absence of lubricant, the thickness distribution numerically obtained with the PC and the CC model together with the experimental results is presented in Fig. 10(i) and (ii). These figures show a gradual thinning in zone I, and a fast thinning at the beginning of zone II, which is also experimentally observed.

As a result of weighting the two frictional mechanisms, the pure viscous and the pure frictional one, the use of the PC model delivers more accurate numerical results than those obtained with the CC model. This can indeed be attributed to the more physics captured by the PC model.

The protrusion height *H* is another important parameter to consider in comparing the performance of lubricants, i.e. the higher is *H* the better is the lubricant (Ngaile et al., 2004b). Fig. 11 shows that the numerical results obtained with the PC model agree quite well with the experimental results. However, a slight discrepancy can be noted in the case of Lub C, with a difference of 29%. This difference can be attributed to the fact that the critical velocity V_{CR}, which marks the passage from a frictional/viscous regime to a pure viscous one, has been assumed to be equal for the three lubricants with $D = 180$ nm for each of them. For the Lub C case, a higher value for V_{CR} appears to be more appropriate so as to longer the development of the frictional/viscous regime, and consequently reduce the tube expansion. Therefore, the assumption of V_{CR} only depending on the lubricant's thickness seems to be too restrictive and should be reconsidered to include the dependence on the lubricant type.

4. Conclusions

A micromechanical motivated frictional/viscous contact model is proposed in this paper to describe boundary lubricated interfaces in the presence of high pressure conditions. The model has been implemented in an explicit FE code and compared with the classical Coulomb's friction law. Unlike the latter, the proposed model was able to reproduce the experimental observations obtained with different lubricants, in particular, the final wall thickness distribution and the protrusion height in a pear-shaped expansion test. The numerical simulations of this test have also shown that the classical Coulomb's model does not reproduce either the friction increase at very slow sliding velocities, or the so called melting effect due to an increasing sliding velocity near the expansion zone. Both the effects were captured by the proposed model.

This has been possible because of the introduction of a parameter α, which depends on the lubrication film thickness *D* and on the sliding velocity *V* and accounts for the different lubrication regimes developed during such process: a pure frictional, a pure viscous and an intermediate regime.

The linear dependence of the parameter α with the film thickness *D* is an initial attempt to include the lubricant thickness in a lubrication model. Nevertheless, closer approximations to the real behaviour could be considered.

The proposed contact law is thermodynamically consistent and reduces to the model proposed in Ref. (Carlson and Batista, 1996) for 1D steady state sliding. Finally, for a proper calibration of the model parameters, a boundary lubrication map like the one proposed in Ref. (Luengo et al., 1996) would be necessary.

In summary, it can be said that in order to reproduce the different lubrication systems in THF processes, the use of friction models with more physics can be a viable solution. However, there are also other physical and numerical aspects related to the simulation of the workpiece and tools used in the forming process that should also be considered. This paper has focused on the physic of the friction phenomenon and should be considered as a contribution in this sense.

Acknowledgements

The authors gratefully acknowledge the financial support of CONICET and CIUNT, Argentina. The authors also wish to thank Miss Amelia Campos for the English revision.

REFERENCES

Ahmetoglu, M., Altan, T., 2000. Tube hydroforming: state-of-the-art and future trends. J. Mater. Process. Technol. 98, 25–33.

Carlson, J.M., Batista, A.A., 1996. Constitutive relation for the friction between lubricated surfaces. Phys. Rev. E 53, 4153–4165.

Curnier, A., 1984. A theory of friction. Int. J. Solids Struct. 20, 637–647.

Dohmann, F., Hartl, Ch., 1997. Tube hydroforming research and practical applications. J. Mater. Process. Technol. 71, 174–186.

Fremond, M., 1987. Adhrence des solides. Journal de Mécanique Théorique et Appliquée 6, 383–407.

Geiger, M., Dal Bó, P., Hecht, J., 2005. Improvement of formability in tube hydroforming by reduction of friction with a high viscous fluid flow. Adv. Mater. Res. 6–8, 369–376.

Geiger, M., Dal Bó, P., 2005. Improvement of axial sliding in the tube hydroforming process of long components due the reduction of friction by high viscous fluid flow. In: Esaform Conference, 27–29, April 2005, Cluj-Napoca, Romania, pp. 455–458.

Hsu, S.M., 1997. Boundary lubrication: current understanding. Tribol. Lett. 3, 1–11.

Israelachvili, J.N., 1992. Intermolecular and Surface Forces. Academic Press, London.

Ko, M., 2003. Tribological issues in the tube hydroforming process—selection of a lubricant for robust process conditions for an automotive structural frame part. J. Manuf. Sci. Eng. 125, 484–492.

Laursen, T.A., 2002. Computational Contact and Impact Mechanics. Springer Verlag, Berlin.

Luege, M., 2006. Numerical simulation of forming processes with hydroforming, Ph.D. dissertation (in Spanish), National University of Tucuman, Argentina.

Luege, M., Luccioni, B.M., 2006. Finite strain model for contact interface in forming processes. PAMM 6.
Luengo, G., Israelachvili, J., Granick, S., 1996. Generalized effects in confined fluids: new friction map for boundary lubrication. Wear 200, 328–335.
Luengo, G., Schmitt, F.-J., Hill, R., Israelachvili, J., 1997. Thin film rheology and tribology of confined polymer melts: contrasts with bulk properties. Macromolecules 30, 2482–2494.
Marsden, J.E., Hughes, T.J.R., 1994. Mathematical Foundations of Elasticity. Dover Publisher, New York.
Ngaile, G., Jaeger, S., Altan, T., 2004a. Lubrication in tube hydroforming (THF). Part I. Lubrication mechanisms and development of model tests to evaluate lubricants and die coatings in the transition and expansion zones. J. Mater. Process. 146, 108–115.
Ngaile, G., Jaeger, S., Altan, T., 2004b. Lubrication in tube hydroforming (THF). Part II. Performance evaluation of lubricants using LDH test and pear-shaped tube expansion test. J. Mater. Process. 146, 116–123.
Plancak, M., Vollersten, F., Woitschig, J., 2005. Analysis, finite element simulation and experimental investigation of friction in tube hydroforming. J. Mater. Process. Technol. 170, 220–228.
Ruina, A.L., 1983. Slip instability and state variable friction laws. J. Geophys. Res. 88, 359–370.
STAMPACK®, Simulation software for multi-stage metal forming operations, Quantech, Barcelona, Spain.
Tabor, D., 1952. Mechanism of boundary lubrication. P. Roy. Soc. Lond. Series A 212, 498–505.
Vollersten, F., Plancak, M., 2002. On possibilities for the determination of the coefficient of friction in hydroforming of tubes. J. Mater. Process. Technol. 125–126, 412–420.
Vollersten, F., Prange, T., Sander, M., 1999. Hydroforming: needs, developments and perspectives. Adv. Technol. Plasticity, 1197–1210.
Wriggers, P., 2002. Computational Contact Mechanics. John Wiley & Sons, Chichester.